Journal of Stress Analysis
Vol. 5, No. 2, Autumn − Winter 2020-21, 21-31

Bu-Ali Sina University

ORIGINAL RESEARCH PAPER

Shear Strain Distribution in Cylindrical Samples Subjected to Deformation by Various Routes of Equal Channel Angular Pressing

M. Etemadi, A.M. Rashidi*
Mechanical Engineering Department, Razi University, Kermanshah, Iran.

Article info

Article history:
Received 18 November 2020
Received in revised form
06 February 2021
Accepted 28 February 2021

Keywords:
Analytical modeling
ECAP
Shear strain
Plastic deformation
Route

Abstract

Equal Channel Angular Pressing (ECAP) is an efficient process to produce bulk nanostructured materials, in which a large amount of strain can be imposed on the workpiece via multiple passing deformations without changing its dimensions. In this study the distribution of induced strain was analytically modeled by correlating the Cartesian coordinates with inclination angle (α) and polar angle (θ). The effects of die angles and the routes A and B (without and with rotation 90° around the billet axis) were evaluated. The results indicated that the degree of strain rate for the inner corner was three times higher than that of the outer corner. In deformation via route A, the degree of strain rate for θ changed from pass to pass, but for α was the same for all the applied passes. In comparison, when the sample was subjected to deformation through route B, the strain distribution patterns altered from pass to pass. For route B, the maximum value of the inhomogeneity index was approximately 1.5 times less than that of route A.

Nomenclature

θ	Angular position	s	Distance between the two given points
ϕ	Die inner corner angle	r	Cylindrical sample radius
ψ	Die outer corner angle	γ	Average angle of die corner
β	Average angle of die corner	α	Inclination angle

1. Introduction

Severe Plastic Deformation (SPD) process refers to any method of metal forming under enormous hydrostatic pressure, where a large plastic strain required for exceptional grain refinement is conveyed to a bulk workpiece without causing any damage and significant change in the overall dimension of the workpiece [1]. Over the last few decades, SPD methods have become an attractive investigation practice for many researchers, so more than 10,000 researchers from 80 countries have contributed to improving the investigation of SPD methods [2]. This is due to the fact that the SPD methods are capable of producing high strength and specific properties of bulk ultrafine-grained and nanostructured materials that are well beyond the predicted properties of traditional coarse-grained and moderately deformed materials.

*Corresponding author: A.M. Rashidi (Associate Professor)
E-mail address: rashidi673@yahoo.com
http://dx.doi.org/10.22084/jrstan.2021.22598.1160
ISSN: 2588-2597

Different SPD methods are now available to achieve ultrafine-grained and nanostructured materials, so more than 100 techniques have been applied as SPD processes to date [3]. Among those, the ECAP, also called ECAE (equal channel angular extrusion), is the most popular SPD technique [4]. In this technique, a cylindrical or square sample workpiece is pressed through a die with two channels, equal in cross-section, intersecting at an inner and outer corner angle of ϕ and ψ, respectively (Fig. 1). As a consequence, in a narrow zone parallel to the intersecting plane, the sample is subjected to shear deformation, while its cross-section remains the same after deformation so that the process can be repeated several times. It should be noted that to introduce the required plastic strain for creating ultrafine grains; the deformation process has to be repeated by reintroducing the sample into the die via route A (no rotation), route B (rotation ±90° about the billet axis), and route C (rotation 180° around the longitudinal axis of billet). Detailed information is given in the review article presented by Valiev and Langdon [5].

The severe plastic deformation by the ECAP process leads to grain refinement to the submicrometer or nanometer level with high angle grain boundaries. It simultaneously alters the phase transformation, which in some cases, leads to the creation of unusual phases or inhibits the formation of some phases [6]. These strain-induced phase transformations are generally accompanied by considerable volume change. As a result, the probability of damage to ECAP dies can greatly be enhanced due to combined local mechanical deformation and phase transformations during the severe plastic deformation process. Furthermore, strain distribution has a significant effect on achieving homogeneous mechanical and physical properties. All these make it necessary to characterize the strain distribution in the ECAP process and rely on its mathematical modeling.

A most up-to-date, informative summary of the advantages/weaknesses and the conceptual and computational challenges of the various SPD modeling can be found in Ref. [7]. Several efforts have been provided to analyze the distribution of equivalent plastic strain in ECAP using FEM (i.e., Refs. [8, 9]). By considering the effects of motion path and velocity, Zhang et al. [10] recently formulated the shear strain during ECAP. To predict the strain in ECAP, Milind and Date [11] developed various analytical models by the kinematic approach. Narooei and Karimi Taheri [12] used a streamlined approach to the cubic Bezier formulation. An upper-bound approach was used by Payadar et al. [13] for equal channel angular extrusion with a circular cross-section. Beyerlein and Tomé [14] presented a mathematical framework for the plastic deformation and velocity gradients associated with a single pass of the ECAE by representing the Plastic Deformation Zone (PDZ) as a two-part PDZ consisting of a central fan-like in the 'upper' region and low-intensity shear deformation in the lower region.

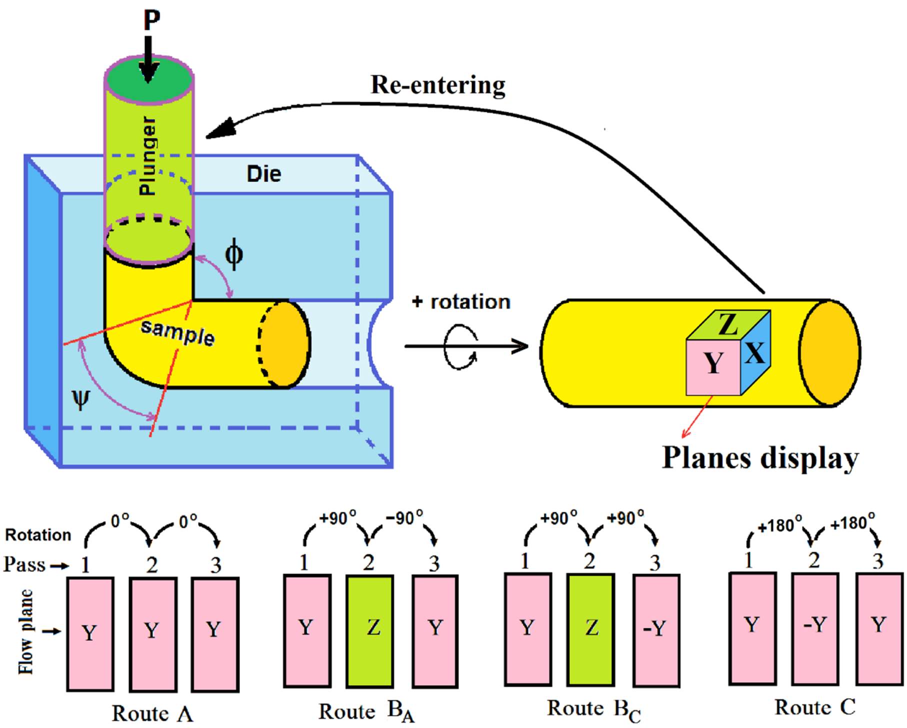

Fig. 1. Schematic illustration of ECAP facility, showing the transverse $(X, -X)$, flow $(Y, -Y)$, and longitudinal $(Z, -Z)$ planes as well as the position changing of $Y(-Y)$ and $Z(-Z)$ planes during the repetition of passes with routes A, B_A, B_C, and C.

Segal [15] used the slip line method to evaluate the strain distribution in ECAP. Iwahashi et al. [16] achieved the most commonly used strain prediction model, in which the variance of the effects on induced strain (γ) was analytically modeled as a function of ECAP die geometries (inner and outer corner arc of die curvature). However, along with the local accumulative shear strain imposed along the streamline, the problems of estimating the strain introduced by the various routes of repeated passing deformation (except for route A) have persisted. To reduce these deficiencies without using the Finite Element Method (FEM) simulations and associated complications, the author proposes to confine to extending Iwahashi's geometrical analysis [16] and introducing an analytical approach for calculating the local accumulative shear strain imposed on each point through the various routes of repetitive deformation by ECAP process. In the previous work [17], the initial treatment and the final finding formulas for estimating accumulative shear strain during successive ECAP process with route B_c were presented and used to calculate the amounts of the induced mating surface stretch at different points of copper/steel bimetallic interface. Here, different stages of our efforts are explained in detail for the first time to model a set of factors affecting the accumulative shear strain such as inner and outer corner angles of ECAP die, angular displacements (rotation angular around the longitudinal axis of the sample, θ), the position on the streamline(determined by inclination angle α), the number of repetitive passage, and the deformation routes. Moreover, the strain distribution during the passage of the sample through the die is examined using the obtained relationships and indicated that only at low angles of θ and high angles of α, the die angles effects can be considerable. For comparative analysis of the effect of effective angles and heterogeneity of strain distribution in ECAPed samples, new useful indices have also been introduced. The research worker will benefit from these models and indices to estimate the position where the strain-induced phase transition is initiated during repeated deformation and to introduce appropriate modifications to ECAE die characteristics so that its likelihood of damage is reduced to the minimum possible degree.

2. Materials and Methods

2.1. Derivation of a Basic Formula

In engineering usage, the strain is referred to as the amount of any relative displacements (rotation, translation, and both) between two presumed points A and B in a body. As they pass along streamlines in the PDZ, the shear strain is associated with the Path Difference (PD) between two given points, which is given by [11]:

$$\gamma = \frac{PD}{s_0} \tag{1}$$

where s_0 is equal to the initial distance between the given points before entering the PDZ. Therefore, the derivation of the relationship between the path difference and the location coordinates of any particle in the PDZ is essential for the assessment of shear strain distribution.

Here, we define three separate orthogonal planes: the transverse plane (X) perpendicular to the flow direction, the flow plane (Y) parallel to the side face, and the longitudinal plane (Z) parallel to the top surface of the sample. These planes are illustrated in Fig. 1. Furthermore, the rounded corner die is considered with cylindrical channels and the PDZ is divided into the three distinct zones I, II, and III, (Fig. 2a). The streamlines, which are straight lines in I and III zones and curved shapes are in the middle region (zone II). Fig. 2b shows the position of an assumed particle "A" at its initial location to start entering to PDZ (marked as "1") and after its displacement on the streamline in zone I (denoted as "2").

By referring to Fig. 2, the Cartesian coordinates of "A" locations can be correlated to θ (angular position around the center flow axis or entry die centerline), α (inclination angle of transverse plane to the longitudinal plane in PDZ), and r (distance from the center flow axis) as the following forms:

$$x_{A1} = x_{A2} = r\cos\theta \tag{2}$$

$$y_{A1} = y_{A2} = r\sin\theta \tag{3}$$

$$z_{A1} = 0, \quad \text{and}$$

$$z_A = z_{A2} = (r - x_{A2})\tan\alpha = r(1-\cos\theta)\tan\alpha \tag{4}$$

Then, point "B" is considered at the position of $\theta+\delta\theta$ and r at the beginning of entering PDZ, as well as at the location of $\theta+\delta\theta$, r, and α on the streamline after its displacement (Fig. 2b), respectively. The initial distance between "A" and "B" can be expressed as $s_o = r\delta\theta$. Given the fact that the value of $\delta\theta$ is minimal such that $\sin\delta\theta = \delta\theta$ and $\cos\delta\theta = 1$, the Eqs. (2) to (4) can be rewritten for particle "B" as follows:

$$\begin{aligned} x_{B1} = x_{B2} &= r\cos(\theta+\delta\theta) \\ &= r(\cos\theta\cos\delta\theta - \sin\theta\sin\delta\theta) \\ &= r\cos\theta - s_o\sin\theta \end{aligned} \tag{5}$$

$$\begin{aligned} z_{B1} = 0, \quad \text{and} \quad z_B = z_{B2} &= (r - x_{B2})\tan\alpha \\ &= r(1-\cos\theta)\tan\alpha + s_0\sin\theta\tan\alpha \end{aligned} \tag{6}$$

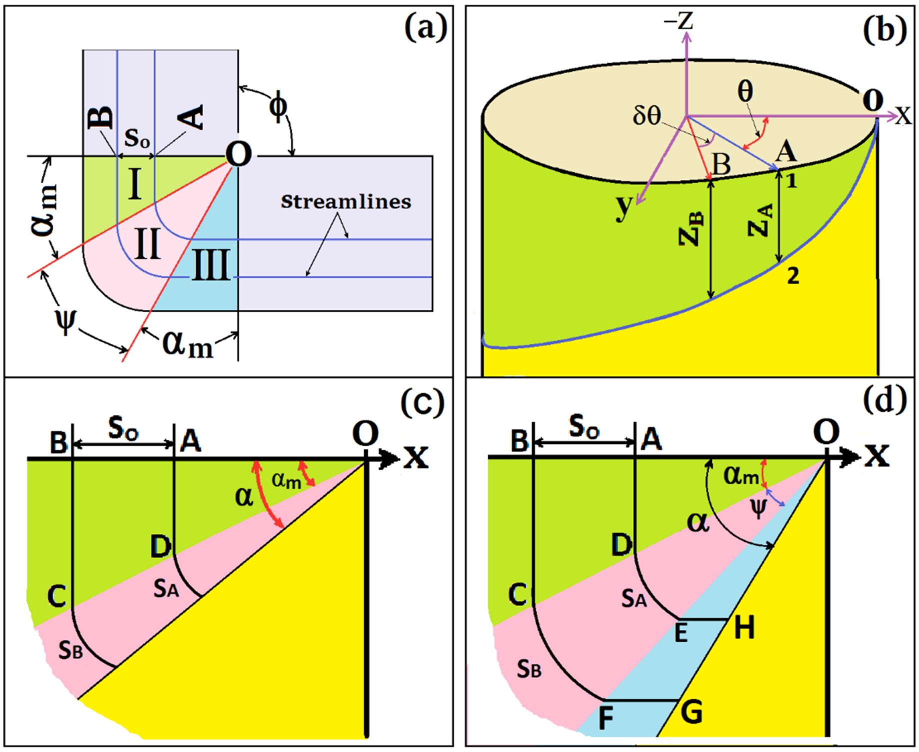

Fig. 2. Schematic representation of plastic deformation zones and streamlines (a), and relations between Cartesian coordinates of the given A and B particles with their angular position (θ) and inclination angle (α) in the regions I (b), II (c), and III (d).

Thus, the path difference in the zone I can be expressed as:

$$PD = |z_B - z_A| = |s_o \sin\theta \tan\alpha| \quad (7)$$

Considering Eq. (1), the accumulative shear strain imposed on any point of the region of I during the first pass can be given as:

$$\gamma_1 = |\sin\theta||\tan\alpha| \quad (8)$$

Fig. 2c shows a schematic illustration of the positions of the given A and B particles in region II at an inclination angle of α. Accordingly, the expressions for the path difference would be:

$$\begin{aligned} PD &= |(BC + s_B) - (AD + s_A)| \\ &= |(BC - AD) + (s_B - s_A)| \end{aligned} \quad (9)$$

From Fig. 2a, $\alpha_m = \pi/(2-\beta)$, where $(\beta = (\phi+\psi))/2$, so referring to Eq. (7), it can be written:

$$BC - AD = s_o \sin\theta \tan\alpha_m = s_0 \sin\theta \cot\beta \quad (10)$$

Referring to Fig. 2c, $s_B - s_A$ can be given as:

$$\begin{aligned} s_B - s_A &= (OC - OD)(\alpha - \alpha_m) \\ &= (OC - OD)(\alpha + \beta - \pi/2) \end{aligned} \quad (11)$$

And

$$\begin{aligned} OC - OD &= (r - x_B)/\cos\alpha_m - (r - x_A)/\cos\alpha_m \\ &= (x_A - x_B)/\cos\alpha_m = s_0 \end{aligned} \quad (12)$$

As a result:

$$s_B - s_A = (\alpha + \beta - \pi/2)s_o \sin\theta \ \mathrm{cosec}\beta \quad (13)$$

Hence, Eq. (9) can be rewritten as:

$$PD = |s_o \sin\theta||\cot\beta + (\alpha + \beta - \pi/2)\mathrm{cosec}\beta| \quad (14)$$

Thus, regarding Eq. (1), γ_{II} can be written as the following function:

$$\gamma_{II} = |\sin\theta||\{\cot\beta + (\alpha + \beta - \pi/2)\mathrm{cosec}\beta| \quad (15)$$

A schematic illustration of the A and B positions at the inclination angle of α in the region III is shown in Fig. 2d. Accordingly, the path difference can be given as:

$$PD = |PD_{s,III} + FG - EH| \quad (16)$$

The $PD_{s,III}$ is the path difference between A and B points where $\alpha = \alpha_m + \psi = \pi/(2-\beta) + \psi$. Referring to Eq. (14), it can be expressed as:

$$PD_{s,III} = |s_0 \sin\theta||\cot\beta + \psi\mathrm{cosec}\beta| \quad (17)$$

On the other hand, by similar treatment as above, it can be obtained that:

$$FG - EH = |s_0 \sin\theta||\cot\beta + \tan(\alpha + \phi)| \quad (18)$$

Thus, the accumulative shear strain in the III region (γ_{III}) is formulated as:

$$\gamma_{III} = |\sin\theta||\{2\cot\beta + \psi\cdot \mathrm{cosec}\beta + \tan(\alpha+\phi)\}| \tag{19}$$

Finally, the total shear strain induced in the first pass (γ_{t1}) can be accounted from Eq. 19, where α is equal to $\pi-\phi$. Thus,

$$\gamma_{t1} = |\sin\theta||(2\cot\beta + \psi\cdot \mathrm{cosec}\beta)| \tag{20}$$

The importance of Eqs. (8), (15) and (19) is that they can be used to examine how the accumulative shear strain is distributed on selected regions over the periphery of an assumed circular with radius r during the deformation of cylindrical samples by the ECAP process. These equations, however, are only valid for the first deformation passage of the ECAP process since the equations are written on the premise that the ECAP process is carried out on the strain-free sample. Although varying quantities of strain have been expended on the various workpiece points, deformation is performed in successive ECAP test passes.

2.2. Deformation History Impact

To address the deformation history effect on the distribution of accumulative shear strain, the followings are considered in the new pass:

(a) The angular position of the given point "A" differs from the previous one by the amount of $0, \pm\pi/2$ and π, depending on the applied deformation routes as indicated in Fig. 1.

(b) The cumulative shear strain is equal to the sum of the total strain induced in the previous passes and calculated from the Eqs. (8), (15) and (19) using the new angular position instead of θ.

The angular position is always equal to θ for deformation with route A, and the total strain induced in the first pass is equal to γ_{t1} (Eq. (20)). So, for the second pass deformation with route A, the accumulated imposed shear strain in I, II, and III zones can be formulated as a function of θ and α according to the following relations:

$$\gamma_{I,A2} = |\sin\theta|(2\cot\beta + \psi\cdot \mathrm{cosec}\beta) + \tan\alpha| \tag{21}$$

$$\gamma_{II,A2} = |\sin\theta|\{|(2\cot\beta + \psi\cdot \mathrm{cosec}\beta)| + |\{\cot\beta + \left(\alpha+\beta-\frac{\pi}{2}\right)\mathrm{cosec}\beta)\}|\} \tag{22}$$

$$\gamma_{III,A2} = |\sin\theta|\{|(2\cot\beta + \psi\cdot \mathrm{cosec}\beta)| + |\{2\cot\beta + \psi\cdot \mathrm{cosec}\beta + \tan(\alpha+\phi)\}|\} \tag{23}$$

The total shear strain induced during the first two passes deformation by route A (γ_{t2A}) can be accounted for from Eq. (23), where the α is equal to $\pi-\phi$. Thus,

$$\gamma_{t2A} = 2|\sin\theta(2\cot\beta + \psi\cdot \mathrm{cosec}\beta)| \tag{24}$$

So, for the third pass, the accumulated shear strain created in I, II, and III zones vary with θ and α according to the following relations:

$$\gamma_{I,A3} = |\sin\theta|\cdot\{|4\cot\beta + 2\psi\cdot \mathrm{cosec}\beta| + |\tan\alpha|\} \tag{25}$$

$$\gamma_{II,A_3} = |\sin\theta|\cdot\{|\cot\beta + (\alpha+\beta-\pi/2)\mathrm{cosec}\beta| + |4\cot\beta + 2\psi\cdot \mathrm{cosec}\beta|\} \tag{26}$$

$$\gamma_{III,A_3} = |\sin\theta|\cdot\{|2\cot\beta + \psi\cdot \mathrm{cosec}\beta + \tan(\alpha+\phi)| + |4\cot\beta + 2\psi\cdot \mathrm{cosec}\beta|\} \tag{27}$$

The new angular position is equal to $\frac{\pi}{2}+\theta$ for the second pass deformation with both routes B_A and B_C, and the total strain induced in the first pass is equal to γ_{t1} (Eq. (20)). So, the dependence of the cumulative shear strain on the θ and α in I, II and III zones during second pass deformation with both routes are determined as:

$$\gamma_{I,B2} = |\sin\theta(2\cot\beta + \psi\cdot \mathrm{cosec}\beta)| + \left|\sin\left(\frac{\pi}{2}+\theta\right)\tan\alpha\right| \Rightarrow$$

$$\gamma_{I,B2} = |\sin\theta(2\cot\beta + \psi\cdot \mathrm{cosec}\beta)| + |\cos\theta|\tan\alpha \tag{28}$$

$$\gamma_{II,B_2} = |\sin\theta(2\cot\beta + \psi\cdot \mathrm{cosec}\beta)| + \left|\sin\left(\frac{\pi}{2}+\theta\right)\{\cot\beta + (\alpha+\beta-\frac{\pi}{2})\mathrm{cosec}\beta\right| \Rightarrow$$

$$\gamma_{II,B_2} = |\sin\theta(2\cot\beta + \psi\cdot \mathrm{cosec}\beta)| + \left|\cos\theta\{\cot\beta + (\alpha+\beta-\frac{\pi}{2})\mathrm{cosec}\beta\right| \tag{29}$$

$$\gamma_{III,B_2} = |\sin\theta(2\cot\beta + \psi\cdot \mathrm{cosec}\beta)| + \left|\sin\left(\frac{\pi}{2}+\theta\right)\{2\cot\beta + \psi\cdot \mathrm{cosec}\beta + \tan(\alpha+\phi)\}\right| \Rightarrow$$

$$\gamma_{III,B_2} = |\sin\theta(2\cot\beta + \psi\cdot \mathrm{cosec}\beta)| + |\cos\theta\{2\cot\beta + \psi\cdot \mathrm{cosec}\beta + \tan(\alpha+\phi)\}| \tag{30}$$

The new angular position is equal to θ and π for the third pass deformation with the routes B_A and B_C, respectively, and the total strain induced in the two previous stages is equal to (γ_{t2B}) which is calculated from Eq. (30), where the α is equal to $\pi-\phi$:

$$\gamma_{t2B} = |2\cot\beta + \psi\cdot \mathrm{cosec}\beta|\cdot(|\cos\theta| + |\sin\theta|) \tag{31}$$

On the other hand, the absolute amounts of calculated strains using the angular position of π in the Eqs. (8), (15), and (19) for the B_C route are the same values obtained by using the angular position of θ for the route of B_A. Therefore, the accumulated shear strain during third pass ECAP with routes B_A and B_C is a function of θ and α according to the following relations:

$$\gamma_{I,B_3} = |2\cot\beta + \psi \cdot \mathrm{cosec}\beta| \cdot (|\cos\theta| + |\sin\theta|) + |\sin\theta\tan\alpha| \tag{32}$$

$$\gamma_{II,B_3} = |2\cot\beta + \psi \cdot \mathrm{cosec}\beta| \cdot (|\cos\theta| + |\sin\theta|) + |\sin\theta\{\cot\beta + (\alpha+\beta-\frac{\pi}{2})\mathrm{cosec}\beta\}| \tag{33}$$

$$\gamma_{III,B_3} = |2\cot\beta + \psi \cdot \mathrm{cosec}\beta| \cdot (|\cos\theta| + |\sin\theta|) + |\sin\theta\{2\cot\beta + \psi\cdot\mathrm{cosec}\beta + \tan(\alpha+\phi)\}| \tag{34}$$

In the above equations, It is tried to extract the formulas for the second and third passes of deformation routes of A and B. A similar method can also be applied for higher passes and other routes.

3. Results and Discussion

First, in this section, the early expressions given by Iwahashi et al. [16] and Segal [18] are extracted from the current framework. In the next step, the approach is used to deduce the influence of ECAP parameters like the number of passes and applied deformation routes on the distribution of induced shear strain.

3.1. Comparison with Previous Basic Models

The two basic models for estimating the shear strain induced during the ECP process are proposed by Segal [18] and Iwahashi et al. [16]. Both models can be extracted from general equations established in the previous section. Inspection shows that Eqs. (19), (23), and (27) are reduced to Eqs. (33), (34), and (35), respectively, when $\theta = \dfrac{\pi}{2}$ and $\alpha = \pi - \phi$:

$$\gamma_{A1} = |\left(2\cot\left(\frac{\phi}{2}+\frac{\psi}{2}\right) + \psi\cdot\mathrm{cosec}\left(\frac{\phi}{2}+\frac{\psi}{2}\right)\right)| \tag{35}$$

$$\gamma_{A2} = 2|2\cot\left(\frac{\phi}{2}+\frac{\psi}{2}\right) + \psi\cdot\mathrm{cosec}\left(\frac{\phi}{2}+\frac{\psi}{2}\right)| = 2\gamma_{A1} \tag{36}$$

$$\gamma_{A3} = 3|2\cot\left(\frac{\phi}{2}+\frac{\psi}{2}\right) + \psi\cdot\mathrm{cosec}\left(\frac{\phi}{2}+\frac{\psi}{2}\right)| = 3\gamma_{A1} \tag{37}$$

By considering the Eqs. (35) to (37), it can be concluded that the same shear strain is accumulated in each pass. Thus, the total accumulated shear strain after N passes deformation with route A is equal to:

$$\gamma_{An} = N|2\cot\left(\frac{\phi}{2}+\frac{\psi}{2}\right) + \psi\cdot\mathrm{cosec}\left(\frac{\phi}{2}+\frac{\psi}{2}\right)| = N\gamma_{A1} \tag{38}$$

Eq. (38) is the same as the one presented by Iwahashi et al. [16]. Alternately, when the assumptions are made to $\theta = \dfrac{\pi}{2}$, $\alpha = \pi - \phi$, $\psi = 0$, and $N = 1$, the resulting works out to:

$$\gamma_{A1} = 2\cot\left(\frac{\phi}{2}\right) \tag{39}$$

which is the same as that proposed by Segal [18].

3.2. Inner and Outer Corner Angles Effects

The impact of the inner and outer corner angles of ECAP die on the final cumulative shear strain imposed by the ECAP process was studied by several researchers [13-16,18,19] which showed that these parameters have significant effects. Here, more focus was concentrated on the shear strain distribution rather than the final induced strain and show that the effects of the inner and outer corner angles on the accumulated shear strain are functions of the angular positions (θ) and inclination angle (α).

Eq. (8) shows that for $\alpha \leq 90° - \beta$, namely in I region (Fig. 3a) the amount of local accumulated shear strain is essentially independent of the die geometry. In zones II and III, the effects of the inner and outer corner angles of ECAP die increases by increasing the inclination angle. Using Eqs. (15) and (19), the accumulated shear strain along with the local coordinates θ and $\alpha > 90° - \beta$ is computed and plotted via Matlab software for the first pass deformation by ECAP dies with various inner and outer corner angles. The type of obtained 3D plot is shown in Fig. 3.

As seen, the die angle effects are considered only in the locations with low angles of θ and high angles of α. For example, due to the changing ϕ, ψ from $(90°, 40°)$ to $(110°, 10°)$, the absolute value changes of induced shear strain ($\Delta\gamma$) are about 8.6×10^{-3} and 1.4×10^{-2} when the investigated positions on samples are changed from $(\alpha = 70°, \theta = 30°)$ to $(\alpha = 30°, \theta = 70°)$, respectively. As shown, the value change of induced shear strain is due to variation of die geometry parameters . As can be seen, the amount of strain change at a high θ and low α was more than 1.6 greater than its value at a low θ and high α.

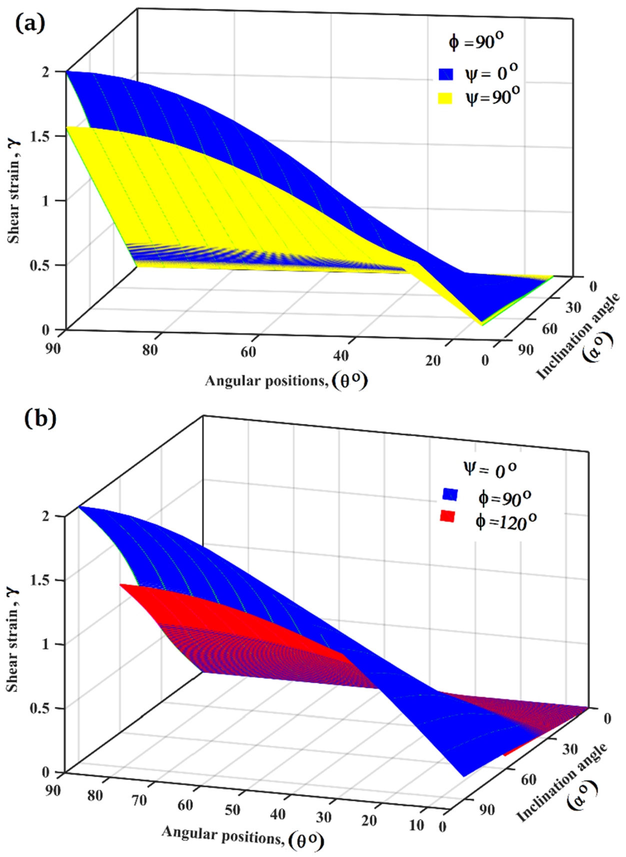

Fig. 3. Variation of induced shear strain with the angular positions (θ) and inclination angle (α) during the first passage through the dies with (a) $\phi = 90°$, $\psi = 0°$ (blue colored graph) and $\phi = 90°$, $\psi = 90°$ (yellow colored graph), (b) $\phi = 90°$, $\psi = 90°$ (blue colored graph) and $\phi = 120°$, $\psi = 0°$ (red colored graph).

Here, the "degree strain rate" (denoted by $\gamma°$") is introduced as a new suitable criterion for evaluating the effect of the inner corner, outer corner, inclination and angular angles of ECAP die on the induced shear strain during the ECAP process. We defined this parameter as $\gamma° = \dfrac{\Delta\gamma}{\Delta\vartheta}$, where ϑ can be ϕ, ψ, α or θ. The "degree strain rate" represents the change in shear strain magnitude when the change of investigated angle is equal to the angular unit.

The peak of shear strain decreased from 2 to about 1.56, as the ψ increased from zero to maximum value 90° under $\phi = 90°$ or the ϕ enhanced from 90° up to 120° under $\psi = 90°$. This means that the average absolute value of the $\gamma°$ for the corner angle variation, namely $|\bar{\gamma}°| = |\dfrac{\Delta\gamma}{\Delta\phi}| = \dfrac{0.44}{\pi/6}$ was about three times higher than that of its value for ψ angle ($|\bar{\gamma}°| = |\dfrac{\Delta\gamma}{\Delta\psi}| = \dfrac{0.44}{\pi/2}$).

The total shear strain in the position of θ, which is induced during the first pass of ECAP deformation, $\gamma_{t1,\theta}$, can be calculated from an extracted formula using $\alpha = 90° - \phi$. It is related to equivalent strain, ε_{eq}, as $\varepsilon_{eq} = \gamma_{t1,\theta}\sqrt{3}$. Fig. 4 provided a simple visual understanding of the significance of the ECAP die inner(channel) angle, ϕ, on the calculated equivalent strain for several curvature angles (ψ) in angular positions of $\theta = 30°$ and $\theta = 90°$. This figure indicated that the induced strain is independent of outer angle ψ in die with an inner angle larger than 90°. These results are in good agreement with the conclusions made by [5, 16, 20].

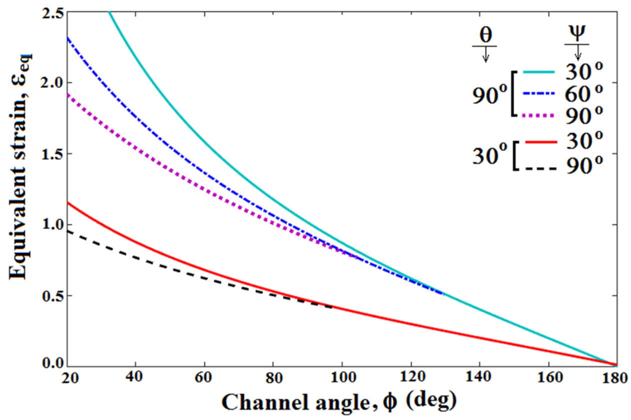

Fig. 4. Illustration of equivalent strain variation with the iner angle of ECAP die for the outer angle of 30°, 60°, 90° and angular position of 30° and 90°.

3.3. Inclination Angle and Angular Positions effects

Fig. 3 illustrates that the variation of induced shear strain along streamlines in PZD (corresponding to inclination angles) is strongly dependent on the angular positions in the transverse plane so that the value of shear strain does not change much at $\theta = 0$ but in the position of $\theta = 90°$, its level increased siginficantly from zero to more than 1.5 with the increase of inclination angle from zero to a maximum amount. Fig. 4 showed that the dependence of the strain imposed on the sample on the angle φ during the first pass of ECAP is highly dependent on the angular location. As described in Section 3.1, the expressions developed in this study well agreed with those developed by Iwahashi et al. [16], when $\theta = \dfrac{\pi}{2}$ and $\alpha = \pi - \phi$. The upper curves corresponding to $\theta = 90°$ in Fig. 4 satisfied these conditions. From the comparison of the upper and lower sets of curves, it can be concluded that the Iwahashi model [16] is an upper-bound analysis for estimating induced strain, which occurred at an angular position of to $\theta = 90°$, while the developed expressions show more details of strain in any locations of samples imposed during ECAP process.

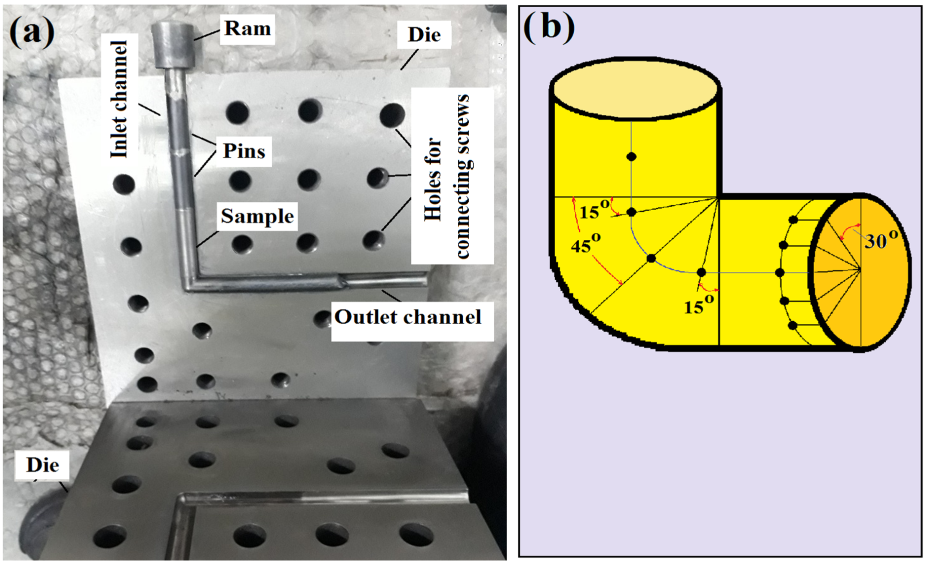

Fig. 5. a) Opened die after pressing sample into its channels, b) Position of selected points for microhardness testing.

It is well known that the effective strain induced during cold working leads to increasing hardness of metallic components based on power form $H = H_o + \varepsilon_{eq}^n$ [21-25]. Microhardness calculation is therefore an effective practical way of determining the impact of ECAP process parameters on the strain induced. Here, in order to evaluate the impact of angular position and inclination angle, the annealed cylindrical sample of low carbon steel AISI1010 with the 100mm length and 9.5mm diameter underwent an ECAP process via die with the inner angle of $\phi = 90°$ and an outer curvature corner angle of $\psi = 30°$. The surfaces of the die channel and samples were completely coated with a MoS_2 lubricant and the ECAP process was performed at room temperature with a ram speed of 20mm/min. After passing a part of the sample through the deformation zones I, II and III (Fig. 2a), the compression of the sample was stopped, the die was opened (Fig. 5a) and the sample was taken out of it. The surface of the sample was cleaned and polished. Then, the microhardness of samples was measured in several locations of streamline and angular positions shown in Fig. 5b using the Vickers indenter. The obtained results are presented in Fig. 6. The variation of microhardness predicted various effective strains plotted in Fig. 7. As seen, the predicted strain dependency of hardness has well followed the power law.

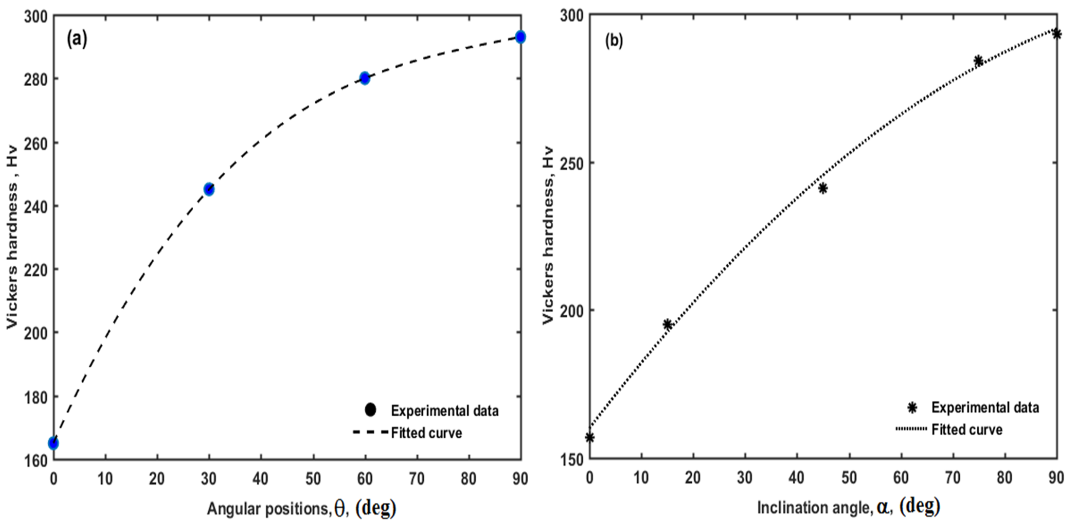

Fig. 6. Variation of microhardness variouse a) Angular position and b) Inclination angle in low carbon steel subjected to ECAP by die with inner angle of $\phi = 90°$ and an outer curvature corner angle of $\psi = 30°$.

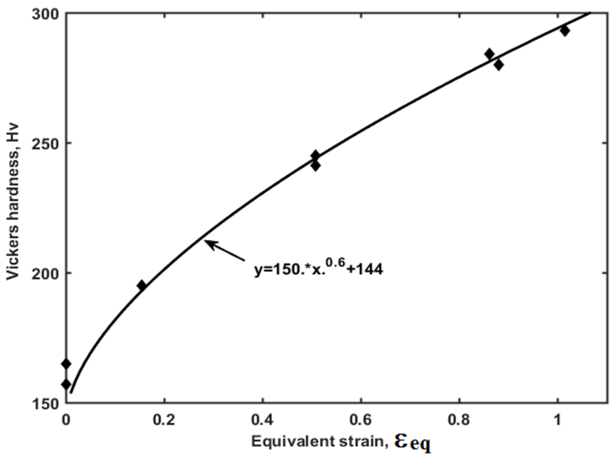

Fig. 7. Demonstrate the power relationship between experimental hardness of ECAPed low carbon steel and predicted equivalent strain induced by die with inner angle of $\phi = 90°$ and an outer angle of $\psi = 30°$.

3.4. Effects of Routes and Successive Passages

Fig. 8 shows the comparison of the patterns of shear strain distribution for the samples subjected up to three successive passes through the ECAP die with $\phi = 90°$ and $\psi = 30°$ by routes A and B.

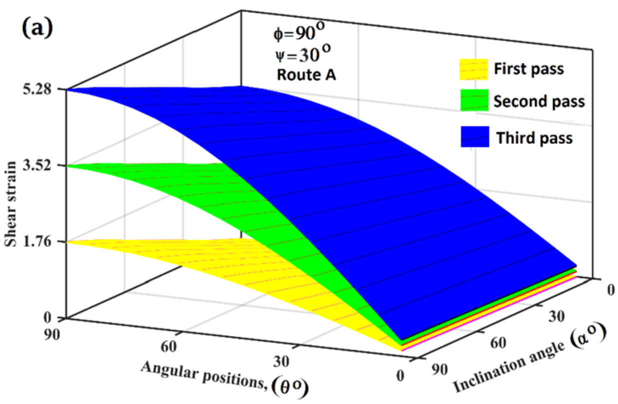

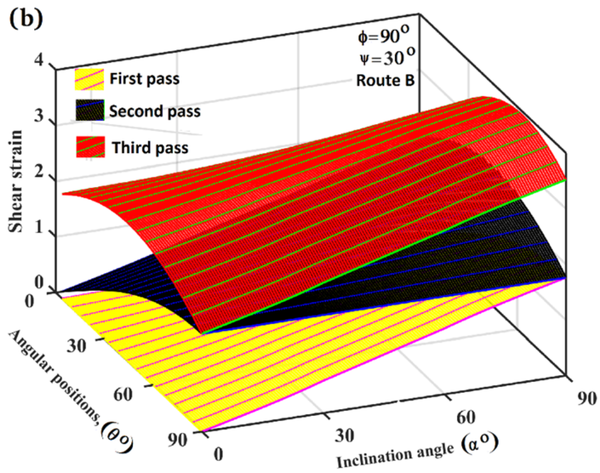

Fig. 8. Variation of induced shear strain with the angular positions (θ) and inclination angle (α) during three passes with (a) route A, (b) route B.

As seen in Fig. 8a, the degree of strain rate for angular positions $\left(\dfrac{\partial\gamma}{\partial\theta}\right)$ considerably changed by changing of passes, but the degree of strain rate for the inclination angle $\left(\dfrac{\partial\gamma}{\partial\alpha}\right)$ and the patterns of shear strain distribution were the same for all applied passes via route A. In contrast, the patterns of shear strain distribution changed from pass to pass when the sample was subjected to repetitive passing deformation via route B, as illustrated in Fig. 8b. Moreover, the maximum shear strain is always created at location coordinates of $\theta = 90°$ and $\alpha = 90°$ for all applied passes via route A, while its location coordinates varied from pass to pass for deformation by route B. Moreover, the difference between the minimum and maximum values of accumulated imposed strain in the third pass deformation with route A which is about 2.3 times higher than that of the value obtained for the same pass with route B.

3.5. Investigation of Inhomogeneity Deformation

An inhomogeneity index was introduced as a ratio of the difference between the maximum and minimum values per the average value of equivalent plastic strains to evaluate the degree of inhomogeneity deformation, [26-29]. Here, this definition is modified as follows:

$$IS = \delta\gamma_i \cdot /\delta\theta_i = (\gamma_{t,i+1} - \gamma_{t,i} \cdot /(\theta_{i+1} - \theta_i) \qquad (40)$$

where $\gamma_{t,i}, \gamma_{t,i+1}$ and IS are the amounts of total accumulated shear strains and the inhomogeneity index in the angular positions of θ_i, θ_{i+1}, and $\theta = (\theta_{i+1} + \theta_i)2$, respectively.

The variations of the $\gamma_{t,i}$ imposed by three passes deformation with routes A and B, as well as their corresponding inhomogeneity indexes, various angular positions are plotted in Fig. 9a and 9b, respectively. It can be clearly seen that when the materials are deformed with route B, the difference between the maximum and minimum values of induced plastic strains is lower than that of the route A. Fig. 9a indicates that although the maximum value of induced shear strains during three passes deformation with route A is about 34% higher than that obtained value for route B, the average values of imposed shear strains (determined as $\bar{\gamma} = 2\left(\int_0^{\pi/2} \gamma_{t,i} d\theta\right)/\pi$) for both deformation routes are approximately the same (∼3.36). On the other hand, the maximum value of the inhomogeneity index for route B is about 1.5 times less than that of its value for route A. This means that the shear strain distribution across the cross-section of the transverse plane perpendicular to the flow direction is more homogeneous when the samples are successively ECAPed with route B in comparison to route A.

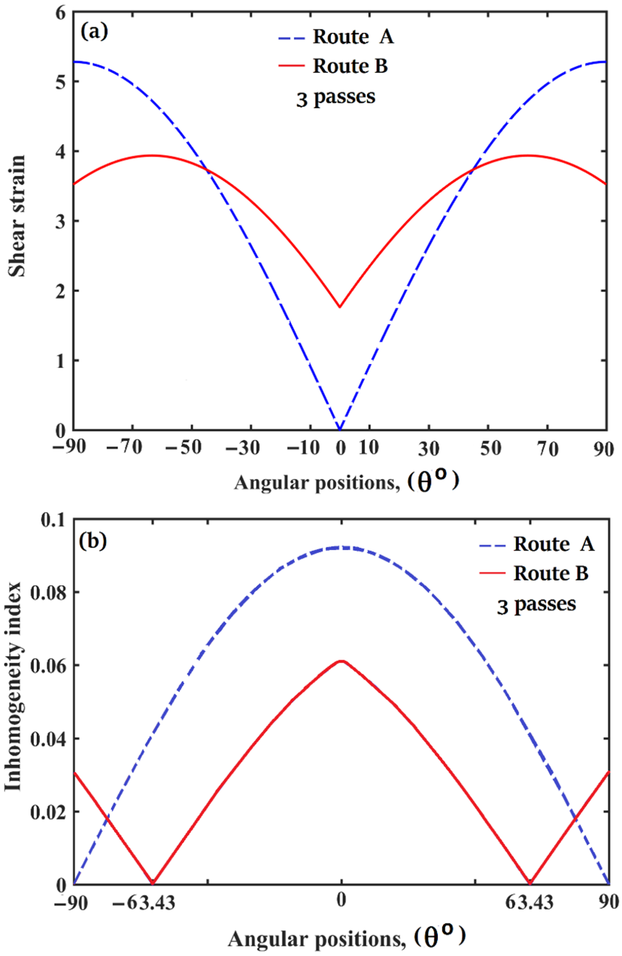

Fig. 9. Variations of a) Induced total shear strain, and b) Inhomogeneity index of shear strain with the angular positions (θ) after three passes with route A and B.

4. Conclusions

In this study, an alternative approach to the derivation of the analytical model for accumulated shear strain distribution in the ECAPed samples was adopted by considering location coordinates as θ (angular position around the center flow axis) and α (inclination angle of transverse plane to the longitudinal plane). The proposed formulas took the history deformation (repetitive passing deformation with various routes) into account, and hence led to more information than those obtained by using Iwahashi's analysis. Additionally, the effect of repetitive passing deformation with routes A and B on the patterns of shear strain distributions were compared. The Following conclusions can be drawn from the findings:

1. The variation of shear strain with α was strongly dependent on θ and the modality of this variation depended on the pass numbers, deformation route and angles of ECAP die.
2. The effect of inner and outer corner angles of ECAP die on strain distribution along the selected local coordinates is considered only in the locations with low angles of θ and high angles of α.
3. The change strain rate for the die inner corner was about three times higher than that of the outer corner.
4. The key differences between route A and route B are the effects of repetitive deformation passes on the shear strain distribution pattern and its inhomogeneity index.
5. The maximum inhomogeneity factor is about 1.5 times less than that of the value of the same index for route A after three deformation passes with route B.
6. The maximum value of induced shear strains during three passes deformation with route A is about 34% higher than the obtained value for route B, but the average values of imposed shear strains for both deformation routes are approximately similar.

Acknowledgment

Authors are grateful to Razi University authority for the support in the present work.

References

[1] Y. Estrin, A. Vinogradov, Extreme grain refinement by severe plastic deformation: a wealth of challenging science, Acta Mater., 61(3) (2013) 782-817.

[2] E. Bagherpour, N. Pardis, M. Reihanian, R. Ebrahimi, An overview on severe plastic deformation: research status, techniques classification, microstructure evolution, and applications, Int. J. Adv. Manuf. Technol., 100 (2019) 1647-1694.

[3] V. Segal, Equal channel angular extrusion (ECAE): from a laboratory curiosity to an industrial technology, Metals, 10(2) (2020) 244.

[4] R. Kapoor, Severe Plastic Deformation of Materials, A.K Tyagi, S. Banerjee, (eds), In: Materials under Extreme Conditions, Recent Trends and Future Prospects, Elsevier Inc, (2017) 717-754.

[5] R.Z. Valiev, T.G. Langdon, Principles of equal-channel angular pressing as a processing tool for grain refinement, Prog. Mater. Sci., 51(7) (2006) 881-981.

[6] B.B. Straumal, A.A. Mazilkin, B. Baretzky, G. Schütz, E. Rabkin, R.Z. Valiev, Accelerated diffusion and phase transformations in CoCu alloys driven by the severe plastic deformation, Mater. Trans., 53(1) (2012) 63-71.

[7] A. Vinogradov, Y. Estrin, Analytical and numerical approaches to modelling severe plastic deformation, Prog. Mater. Sci., 95 (2018) 172-242.

[8] R.B. Figueiredo, M.T.P. Aguilar, P.R. Cetlin, Finite element modelling of plastic instability during ECAP processing of flow-softening materials, Mater. Sci. Eng. A, 430(1-2) (2006) 179-184.

[9] T.D. Horn, C.B. Silbermann, P. Frint, M. Wagner, J. Ihlemann, Strain localization during equal-channel angular pressing analyzed by finite element simulations, Metals, 8 (2018) 55.

[10] D.T. Zhang, Z. Li, Y.X. Tong, Y.F. Zheng, L. Li, New formulas of shear strain during equal-channel angular pressing process with consideration of influences of velocity and motion trajectory, J. Iron. Steel Res. Int., 23(10) (2016) 1020-1027.

[11] T.R. Milind, P.P. Date, Analytical and finite element modeling of strain generated in equal channel angular extrusion, Inter. J. Mech. Sci., 56(1) (2012) 26-34.

[12] K. Narooei, A. Karimi Taheri, A new model for prediction the strain field and extrusion pressure in ECAE process of circular cross section, Appl. Math. Modell., 34(7) (2010) 1901-1917.

[13] M.H. Payadar, M. Reihanian, R. Ebrahimi, T.A. Dean, M.M. Moshksar, An upper-bound approach for equal channel angular extrusion with circular cross-section, J. Mater. Proc. Technol., 198(1-3) (2008) 48-53.

[14] I.J. Beyerlein, C.N. Tomé, Analytical modeling of material flow in equal channel angular extrusion (ECAE), Mater. Sci. Eng. A, 380(1-2) (2004) 171-190.

[15] V.M. Segal, Slip line solutions, deformation mode and loading history during ECAP, Mater. Sci. Eng. A, 345(1-2) (2003) 36-46.

[16] Y. Iwahashi, J. Wang, Z. Horita, M. Nemoto, Principle of ECAE for the processing of UFG materials, Scr. Mater., 35 (1996) 143-146.

[17] A.M. Rashidi, M. Etemadi, Investigation wavy interface forming and stretching in severe plastic deformed copper/steel bimetallic rod, Mech. Adv. Mater. Struct., (2020), DOI: 10.1080/15376494.2020.1747668.

[18] V.M. Segal, Materials processing by simple shear, Mater. Sci. Eng. A, 197(2) (1995) 157-164.

[19] N.E. Mahallawy, F.A. Shehata, M.A.E. Hameed, M.I.A.E. Aal, H.S. Kim, 3D FEM simulations for the homogeneity of plastic deformation in Al-Cu alloys during ECAP, Mater. Sci. Eng. A, 527(6) (2010) 1404-1410.

[20] K. Furuno, H. Akamatsu, K. Oh-ishi, M. Furukawa, Z. Horita, T.G. Langdon, Microstructural development in equal-channel angular pressing using a 60° die, Acta. Mater., 52(9) (2004) 2497-2507.

[21] G.H. Majzoobi, J. Mohammadi, M.K. Pipelzadeh, S. Lahmi, S.J. Hardy, A constitutive model for hardness considering the effects of strain, strain rate and temperature, J. Strain Anal. Eng. Des., 50 (2015) 284-298.

[22] N.A. Branch, G. Subhash, N.K. Arakere, M.A. Klecka, Material-dependent representative plastic strain for the prediction of indentation hardness, Acta Mater., 58(19) (2010) 6487-6494.

[23] F.O. Sonmez, A. Demir, Analytical relations between hardness and strain for cold formed parts, J. Mater. Process. Tech., 186(1-3) (2007) 163-173.

[24] J. Petruska, L. Janicek, On the evaluation of strain inhomogeneity by hardness measurement of formed products, J. Mater. Process. Tech., 143-144(1) (2003) 300-305.

[25] J.H. Palm, The relation between indentation hardness and strain for metals, JOM, 1 (1949) 904.

[26] S.C. Yoon, P. Quang, S.I. Hong, H.S. Kim, Die design for homogeneous plastic deformation during equal channel angular pressing, J. Mater. Process. Tech., 187-188 (2007) 46-50.

[27] R. Naseri, M. Kadkhodayan, M. Shariati, An experimental investigation of casing effect on mechanical properties of billet in ECAP process, Int. J. Adv. Manuf. Technol., 90 (2017) 3203-3216.

[28] S. Li, M.A.M. Bourke, I.J. Beyerlein, D.J. Alexander, B. Clausen, Finite element analysis of the plastic deformation zone and working load in equal channel angular extrusion, Mater. Sci. Eng. A, 382(1-2) (2004) 217-236.

[29] T. Suo, Y. Li, Y. Guo, Y. Liu, The simulation of deformation distribution during ECAP using 3D finite element method, Mater. Sci. Eng., A, 432(1-2) (2006) 269-274.